

Numerically assisted determination of local models in network scenarios

José Mário da Silva* and Fernando Parisio†

Departamento de Física, Universidade Federal de Pernambuco, Recife, Pernambuco 50670-901 Brazil

Taking advantage of the fact that the cardinalities of hidden variables in network scenarios can be assumed to be finite without loss of generality, a numerical tool for finding explicit local models that reproduce a given statistical behaviour was developed. The numerical procedure was then validated using families of statistical behaviours for which the network-local boundary is known, in the bilocal scenario. Furthermore, the critical visibility for 3 notable distributions mixed with a uniform random noise is investigated in the triangle network without inputs. We provide conjectures for the critical visibilities of the Greenberger–Horne–Zeilinger (GHZ) and W distributions (which are roots of 4th degree polynomials), as well as a lower bound estimate of the critical visibility of the Elegant Joint Measurement distribution. The developed codes and documentation are publicly available at github.com/mariofilho281/localmodels.

I. INTRODUCTION

Nonlocality is a hallmark feature of quantum theory that differentiates it from any classical conceptual framework [1]. Soon after Bell’s seminal discovery in 1964, much attention was given to nonlocality in the simplest standard Bell scenario, i.e., a situation where a single source distributes information (classical or quantum) to two parties. Over the years, multipartite scenarios, where one source distributes information to several parties, have also been studied [2–5]. Not only has nonlocality had a profound impact in the foundations of physics, but it also has found application in the field of quantum information [6–9].

The next conceptual leap occurred in 2010 with the introduction of nonlocality in network scenarios [10]. In these scenarios there are several sources, assumed to be independent, distributing information to some of the parties (not all) forming a network topology. All examples of quantum nonlocality in the standard Bell scenarios have a direct analogue in network scenarios [11], but some cases of network-nonlocality do not seem to stem directly from the violation of a Bell inequality in a standard scenario. A fascinating illustration is the occurrence of nonlocality in situations where all parties have no input choices [12]. This may indicate that standard Bell nonlocality is just a specific subset of the more general phenomenon of network-nonlocality, which is far from being completely understood [13].

An important step towards a better understanding of network nonlocality was the demonstration that network-local correlations, with a finite number of inputs and outputs, can *always* be represented by models where the sources distribute hidden variables with finite cardinality, i.e., variables that belong to a finite set of possibilities [14]. A pivotal problem in the field is to know whether a given statistical behaviour is network-local or not. If it is, the referred result guarantees that it can be repro-

duced by a model where the hidden variables only take on a finite number of values. Such models can be represented by finite arrays of real numbers, and therefore can be subjected to optimization algorithms that aim at fitting a local model to the given behaviour.

The purpose of this paper is to present an implementation of this idea, as well as the results we obtained when applying the procedure to certain statistical behaviours in the bilocal and triangle network topologies. In these relatively simple scenarios we were able to devise several closed analytical models from the numerical results. The behaviours we consider are not limited to quantum mechanical ones, but may refer to distributions achievable with supraquantum resources.

The structure of this paper is as follows: in section II, the representation of local models with finite hidden variable cardinalities is explained, as well as the general procedure to obtain models for a given statistical behaviour; in section III, the procedure is applied to statistical behaviours in the bilocal scenario; in section IV, the procedure is applied to noteworthy probability distributions in the triangle scenario; in section V we make our final remarks and discuss some possibilities for future work.

II. REPRESENTATION OF LOCAL MODELS

Network scenarios are situations where there are multiple independent sources distributing information to several parties. We start this section by illustrating the distinctive features of these scenarios with a specific example with four parties and two independent sources, see figure 1. Alice and Charles receive information from one of the sources, whereas Dave gets information from the other source. In this example, the only party which receives information from both sources is Bob. In general, all parties have measurement settings, also called inputs. The outputs a, b, c, d have finite cardinalities that will be represented by m_a, m_b, m_c, m_d , and the inputs x, y, z, w also have finite cardinalities, represented by M_a, M_b, M_c, M_d . Throughout the paper, whenever a variable λ has finite cardinality c_λ , it will be assumed to take on

* jose.filho@ufpe.br

† fernando.parisio@ufpe.br

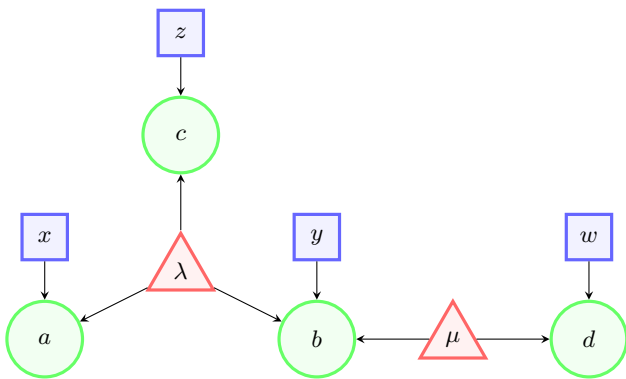


FIG. 1. Example of a network scenario. The outputs of each party, denoted by a , b , c and d , are represented by green circles, while the inputs x , y , z and w are represented by blue squares. The local hidden variables λ and μ are represented by red triangles. A network-local behaviour $p(a, b, c, d|x, y, z, w)$ in such a scenario can always be cast into the form of equation 1 (notice the statistical independence between λ and μ).

values in the set $\{0, 1, \dots, c_\lambda - 1\}$. The statistical behaviour $p(a, b, c, d|x, y, z, w)$ is said to be network-local if and only if there are probability distributions $p_\lambda(\lambda)$, $p_\mu(\mu)$, $p_a(a|x, \lambda)$, $p_b(b|y, \lambda, \mu)$, $p_c(c|z, \lambda)$ and $p_d(d|w, \mu)$, such that

$$p(a, b, c, d|x, y, z, w) = \int d\lambda d\mu p_\lambda(\lambda) p_\mu(\mu) p_a(a|x, \lambda) p_b(b|y, \lambda, \mu) p_c(c|z, \lambda) p_d(d|w, \mu). \quad (1)$$

As mentioned before, in [14] it was proven that that the cardinalities of local hidden variables in networks can always be assumed to be finite. The authors also provide an upper bound for the necessary cardinalities that we reproduce here for completeness. Consider for example the hidden variable λ of figure 1. We begin by identifying the full probability distribution of the network $p(a, b, c, d|x, y, z, w)$ and the probability distribution of the parties not connected to the hidden variable, $p(d|w)$, which in this case is only Dave's. The dimensions of these probability distributions are then calculated using the Collins-Gisin parameterization [15]. Finally, the cardinality upper bound is given by the difference of these two dimensions:

$$c_\lambda \leq \dim \{p(a, b, c, d|x, y, z, w)\} - \dim \{p(d|w)\}. \quad (2)$$

Of course we can always count the deterministic strategies available to parties that only receive λ (Alice and Charles in this example) and bound c_λ even further (similar to what is done in the discussion about the local polytope in [8]):

$$c_\lambda \leq m_a^{M_a}, \quad (3)$$

$$c_\lambda \leq m_c^{M_c}. \quad (4)$$

The lowest number in inequalities (2), (3), and (4) could then be considered the final upper bound on c_λ .

If the hidden variables λ and μ have finite cardinalities c_λ and c_μ , equation 1 reduces to

$$p(a, b, c, d|x, y, z, w) = \sum_{\lambda=0}^{c_\lambda-1} \sum_{\mu=0}^{c_\mu-1} p_\lambda(\lambda) p_\mu(\mu) p_a(a|x, \lambda) p_b(b|y, \lambda, \mu) p_c(c|z, \lambda) p_d(d|w, \mu), \quad (5)$$

and the model can be represented by finite arrays of numbers representing the hidden-variable distributions p_λ , p_μ and the parties response functions p_a , p_b , p_c and p_d . To avoid notation clutter, the arrays will be represented by the same symbols as the distributions, but indexed with brackets, like $p_\lambda[i]$, for example. The hidden variable arrays are just lists of the probabilities that the variable assumes the index value:

$$p_\lambda[i] = P(\lambda = i). \quad (6)$$

For example, a hidden variable characterized by $p_\lambda = [3/4 \ 1/4]$ is one that produces 0 with probability 3/4 or 1 with probability 1/4. Obviously, the last element of the array is not independent of the others because of the normalization condition $\sum_{i=0}^{c_\lambda-1} p_\lambda[i] = 1$. Because of this, only $c_\lambda - 1$ probabilities need to be subjected to the optimization procedure when trying to fit a model to a statistical behaviour, as long as we enforce the inequality constraint $\sum_{i=0}^{c_\lambda-2} p_\lambda[i] \leq 1$ in order to have the last element be a valid probability. Although the optimization procedure only works with $c_\lambda - 1$ elements for a given p_λ , we will provide the full array when reporting specific models in sections III and IV.

The response function arrays need to have more indices, like $p_b[i, j, k, l]$, for the example of figure 1. The convention we adopt is as follows: the output value as the first index, the input value as the second index (if the party has a choice of measurement settings), and the remaining indices being the values of the hidden variables connected to that party.

The generalization of this procedure to arbitrary network architectures is immediate. The response function array of a generic party with output a , input x and hidden variables $\lambda_1, \dots, \lambda_n$ is then defined as:

$$p_a[i, j, k, \dots, l] = P(a = i|x = j, \lambda_1 = k, \dots, \lambda_n = l). \quad (7)$$

Because of the normalization condition in the response function $\sum_{i=0}^{m_a-1} p_a[i, j, k, \dots, l] = 1$, the numerical procedure needs to optimize only $m_a - 1$ probabilities for each combination of inputs and hidden variables. In summary, the number of parameters to optimize are $c_\lambda - 1$ per hidden variable and $(m_a - 1)M_a c_{\lambda_1} \dots c_{\lambda_n}$ per party.

When reporting response functions of parties, we will do so in matrix form, using the second to last index to represent rows and the last index to represent columns. In our example, if Alice's output a is binary, the response function array

$$p_a[0, x, \lambda] = \begin{bmatrix} 1 & \frac{1}{2} \\ \frac{1}{2} & 0 \end{bmatrix}$$

represents a situation where Alice outputs x if $x = \lambda$ or a uniformly distributed random bit if $x \neq \lambda$. The array $p_a[1, x, \lambda]$, being determined by the normalization condition.

Given the hidden-variable arrays p_λ, p_μ, \dots and the party arrays p_a, p_b, \dots , all the probabilities $p(a, b, \dots | x, y, \dots)$ can be calculated:

$$p(a, b, \dots | x, y, \dots) = \sum_{i, j, \dots} p_\lambda[i] p_\mu[j] \dots p_a[a, x, \dots] p_b[b, y, \dots] \dots \quad (8)$$

Therefore, the problem of finding a local model for a given behaviour $p^*(a, b, \dots | x, y, \dots)$ can be reduced to a constrained non-linear optimization problem on the elements of p_λ, p_μ, \dots and p_a, p_b, \dots , with the sum of squared errors in the probabilities as the cost function:

$$\begin{aligned} \min_{\substack{p_\lambda, p_\mu, \dots, \\ p_a, p_b, \dots}} \sum_{\substack{a, b, \dots, \\ x, y, \dots}} [p(a, b, \dots | x, y, \dots) - p^*(a, b, \dots | x, y, \dots)]^2 \\ \text{s.t.} \quad p_\lambda, p_\mu, \dots, p_a, p_b, \dots \geq 0 \\ \sum_i p_\lambda[i] \leq 1 \\ \sum_i p_\mu[i] \leq 1 \\ \dots \\ \sum_i p_a[i, \dots] \leq 1 \\ \sum_i p_b[i, \dots] \leq 1 \\ \dots \end{aligned} \quad (9)$$

where $p(a, b, \dots | x, y, \dots)$ are given by equation 8.

In order to apply this idea to solve interesting problems regarding the bilocal and triangle topologies (figures 2 and 5), two Python modules named `bilocal.py` and `triangle.py` were created. The code and documentation are publicly available at github.com/mariofilho281/localmodels. In these two modules, the optimization problem 9 is solved with a trust-region algorithm for constrained optimization available in the SciPy package [16]. This algorithm deals with inequality constraints by employing the barrier method, which reduces the original problem to a sequence of equality constrained problems. Each of these sub-problems is then solved using a trust-region sequential quadratic programming (SQP) with the projected conjugate gradient (CG) method [17].

One important remark is that in standard Bell nonlocality, the problem of finding a local model for a given behaviour (if one such model exists) is substantially easier. In fact, it reduces to a feasibility problem in linear programming, for which there are algorithms that can provide an explicit model in case the behaviour is local, or a Bell inequality violated by the behaviour in case it

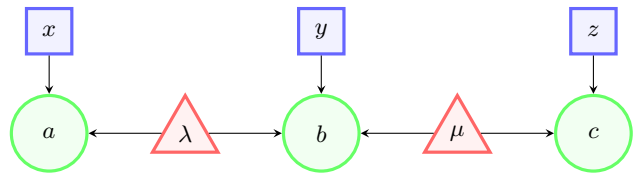


FIG. 2. In the bilocal scenario there are three parties and two sources. Alice (Charles) receives information from source λ (μ). Bob is connected to both sources. In contrast to standard Bell scenarios, the multiple hidden variables are not distributed to all parties and are assumed to be statistically independent.

is not local [9]. In network nonlocality, such methods are not applicable because the problem of finding a network local model is no longer an instance of convex optimization.

The idea of this work is in the same spirit of [18], where the authors propose a machine learning algorithm to find local models for target distributions. These local models have hidden variables with continuous uniform distribution, and all the complexities needed to fit a given behaviour falls onto the parties response functions, given by neural networks. In contrast, our method employs discrete hidden variables (in general not uniformly distributed), which allowed us to find simpler models, some even with closed analytical expressions for the probabilities involved (see section IV).

III. BILOCAL NETWORK

As a first application of the technique, let us consider the problem of finding an approximation for the boundary of the bilocal set in affine subspaces of dimension 2 in the no-signalling space. Following [19], consider the bilocal network (figure 2) with binary inputs and outputs, and define the distributions p_I, p_J and p_0 given by:

$$p_I(a, b, c | x, y, z) = \frac{1}{8} [1 + \delta_{y,0} (-1)^{a+b+c}], \quad (10)$$

$$p_J(a, b, c | x, y, z) = \frac{1}{8} [1 + \delta_{y,1} (-1)^{x+z+a+b+c}], \quad (11)$$

$$p_0(a, b, c | x, y, z) = \frac{1}{8}. \quad (12)$$

The behaviour composed by a convex sum of the previous distributions $p = Ip_I + Jp_J + (1 - I - J)p_0$ (with $|I| \leq 1$ and $|J| \leq 1$) is network local if and only if the so called BRGP inequality [19] is satisfied:

$$\sqrt{|I|} + \sqrt{|J|} \leq 1. \quad (13)$$

By counting the deterministic strategies available to Alice and Charles in the bilocal scenario with 2 possible outputs, we can show that any network-local distribution can be achieved with the hidden variables cardinalities

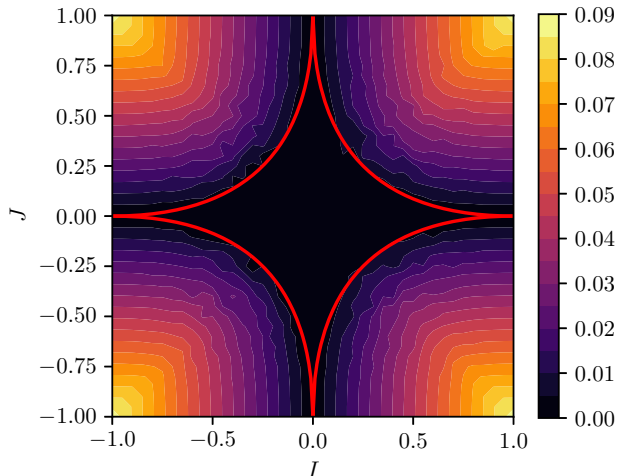


FIG. 3. Optimization error in the affine subspace spanned by the distributions (10) to (12). The solid red line is the bilocal boundary given by the BRGP inequality (13). For behaviours inside the boundary, the solver can get the optimization error close to zero. As we move away from the boundary to behaviours that are not bilocal, the error grows, as expected.

$c_\lambda = c_\mu = 4$ [14]. We solved problem 9 with these cardinalities for a rectangular grid of pairs (I, J) . The optimization error can be seen in figure 3. The optimization error of problem (9) is first divided by 64 [the number of entries in the probability distribution $p(a, b, c|x, y, z)$] and then taken the square root, before being plotted. One can therefore interpret the colour scale of figure 3 as the root mean square error in the probabilities. The solid red line is the boundary of the network-local set in this 2-dimensional slice given by inequality (13). The first thing we notice is that the points inside this region exhibit optimization error close to zero, showing that the solver has found acceptable local models for them. Also, behaviours outside the network-local boundary exhibit higher error, showing that the solver did not find faithful local models for them. This provides a first validation of the method in a known problem.

Now, let us move on to a distinct two-dimensional slice of the behaviour space. Let us define the following conditional distributions:

$$p_X(a, b, c|x, y, z) = \frac{1}{8} \left(\frac{1}{2} + \delta_{a,0} \right) [1 + \delta_{y,0} (-1)^{a+b+c}], \quad (14)$$

$$p_Y(a, b, c|x, y, z) = \frac{1}{8} \left(\frac{1}{2} + \delta_{a,0} \right) [1 + \delta_{y,1} (-1)^{z+a+b+c}], \quad (15)$$

$$p_0(a, b, c|x, y, z) = \frac{1}{8} \left(\frac{1}{2} + \delta_{a,0} \right). \quad (16)$$

For the remainder of this section, we will concern

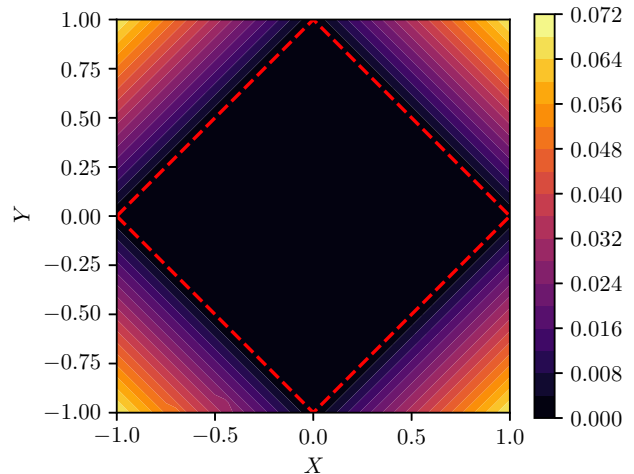


FIG. 4. Optimization error in the affine subspace spanned by the distributions (14) to (16). The red dashed line is the boundary of the bilocal set in this two-dimensional slice of the behaviour space, as proven in the end of this section. For behaviours inside the boundary, the solver can get the optimization error close to zero. As we move away from this region, the error grows, indicating that the behaviours are no longer bilocal.

ourselves with the affine subspace spanned by the distributions (14) to (16), i.e., the set of behaviours $p(a, b, c|x, y, z)$ given by the convex combination

$$p = Xp_X + Yp_Y + (1 - X - Y)p_0, \quad (17)$$

where the dependency on a, b, c, x, y and z has been omitted to keep the notation clean.

The BRGP inequality for this region of the behaviour space reduces to $|X| \leq 1$. Once again, we will work in the domain $X, Y \in [-1, 1]$, but in this case, all the points of the square satisfy the BRGP inequality, which leaves the whole square region as potentially bilocal. Let us check if this is indeed the case. The numerical procedure outlined above was performed for this affine subspace, with problem (9) being solved 50 times for each behaviour, with a density of 420 points per unit area of the XY plane. The optimization error of this procedure can be seen in figure 4 (the red dashed line will be explained shortly).

We see in figure 4 that the solver found acceptable bilocal models only for points in the darker regions of the square domain, illustrating the non tightness of the BRGP inequality in this affine subspace. The square bounded by the red dashed lines in figure 4 is characterized by the following inequality:

$$|X| + |Y| \leq 1. \quad (18)$$

Focusing on the boundary behaviours located in the first quadrant, their probability distribution is given by

$$p(a, b, c|x, y, z) = \frac{1}{8} \left(\frac{1}{2} + \delta_{a,0} \right) [1 + X\delta_{y,0}(-1)^{a+b+c} + Y\delta_{y,1}(-1)^{z+a+b+c}], \quad (19)$$

with $X + Y = 1$. The resulting numeric models close to this line display the noticeable feature that two out of the four possible values of λ have a probability very close to zero. This is an indication that $(c_\lambda, c_\mu) = (2, 4)$ is enough to reproduce these probability distributions. By recalculating the models with these reduced cardinalities, and further noticing that all numerically determined entries are very close to “simple” rational numbers, we were able to devise the following model:

$$p_\lambda[\lambda] = \left[\frac{3}{4} \quad \frac{1}{4} \right], \quad (20a)$$

$$p_\mu[\mu] = \left[\frac{Y}{2} \quad \frac{X}{2} \quad \frac{Y}{2} \quad \frac{X}{2} \right], \quad (20b)$$

$$p_a[0, x, \lambda] = \begin{bmatrix} 1 & 0 \\ 1 & 0 \end{bmatrix}, \quad (20c)$$

$$p_b[0, 0, \lambda, \mu] = \begin{bmatrix} \frac{1}{2} & 1 & \frac{1}{2} & 0 \\ \frac{1}{2} & 0 & \frac{1}{2} & 1 \end{bmatrix}, \quad (20d)$$

$$p_b[0, 1, \lambda, \mu] = \begin{bmatrix} 1 & \frac{1}{2} & 0 & \frac{1}{2} \\ 0 & \frac{1}{2} & 1 & \frac{1}{2} \end{bmatrix}, \quad (20e)$$

$$p_c[z, \mu] = \begin{bmatrix} 1 & 1 & 0 & 0 \\ 0 & 1 & 1 & 0 \end{bmatrix}. \quad (20f)$$

This model indeed reproduces (exactly) the behaviour given by equation (19). Behaviours on the other 3 sides of the square ($X - Y = 1$, $X + Y = -1$ and $X - Y = -1$) can be reproduced by the same model if we perform output and/or input relabellings.

Therefore, we proved that all behaviours on the red dashed lines of figure 4 are bilocal. It turns out that the behaviour at the center $X = Y = 0$ is characterized by a factorized probability distribution

$$p_0(a, b, c|x, y, z) = \left(\frac{1}{4} + \frac{1}{2}\delta_{a,0} \right) \left(\frac{1}{2} \right) \left(\frac{1}{2} \right) = p(a|x)p(b|y)p(c|z).$$

Thus, the projection of the bilocal set onto this affine subspace is star-convex with respect to the center behaviour p_0 , as proven in [19]. Therefore, it follows that all behaviours that satisfy inequality (18) are bilocal.

By applying inequality A2 of [20], to this affine subspace, we can see that inequality (18) is the boundary of the local set, where all parties have access to globally shared randomness. Therefore, since we found more restrictive bilocal models for the behaviours at this boundary it follows that inequality (18) is indeed the boundary of the bilocal set in this affine subspace.

The capability of identifying the boundary of the network-local set in these two cases serves as validation for the methodology we have been employing. Next we will show how the solutions of problem (9) can lead to interesting results in the triangle scenario with no inputs.

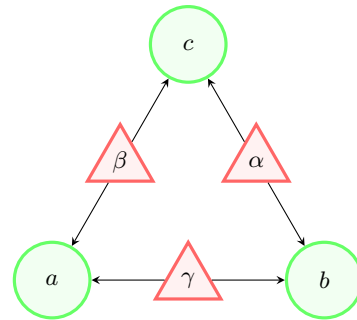


FIG. 5. Triangle scenario with no inputs. The outputs of each party a , b and c are represented by green circles. The local hidden variables α , β and γ are represented by red triangles. Notice the lack of input choices for the parties. This is probably the simplest scenario that exhibits nonlocality without inputs.

IV. TRIANGLE NETWORK

Consider the network scenario depicted in figure 5. This triangle scenario is the simplest network that can exhibit quantum nonlocality without any choice of inputs by the parties. Our goal in the following is to investigate specific regions of the behaviour spaces of two and four output distributions. In subsections IV A and IV B we have $a, b, c \in \{0, 1\}$, while in subsection IV C we have $a, b, c \in \{0, 1, 2, 3\}$. For the triangle scenario with two possible outputs, the cardinality bound in the hidden variables is 6, whereas for the case with four possible outputs it is 60 [14].

A. GHZ distribution

First, let us consider the GHZ distribution, named after the homonymous quantum state [21], mixed with a uniformly distributed random noise:

$$p(a, b, c) = \begin{cases} \frac{v}{2} + \frac{1-v}{8} & \text{if } a = b = c \\ \frac{1-v}{8} & \text{otherwise.} \end{cases} \quad (21)$$

We solved problem (9) for this distribution with the cardinalities $(c_\alpha, c_\beta, c_\gamma) = (2, 2, 2)$, $(3, 2, 2)$, $(3, 3, 2)$, $(3, 3, 3)$ and $(6, 6, 6)$, the latter corresponding to the maximal necessary cardinality. The optimization error as a function of the visibility for each case can be seen in figure 6. The critical visibility increases as we allow for more complex models, as expected, but only up to $(3, 3, 3)$ models. Notice that the results for the triplet $(3, 3, 3)$ typically agree with those of the triplet $(6, 6, 6)$, with some oscillations to the $(3, 2, 2)$ curve. Obviously, this is a numeric artefact that could be eliminated by increasing the number of trials per behaviour.

If we inspect the models for regions close to the critical visibility in each case, several entries in the response

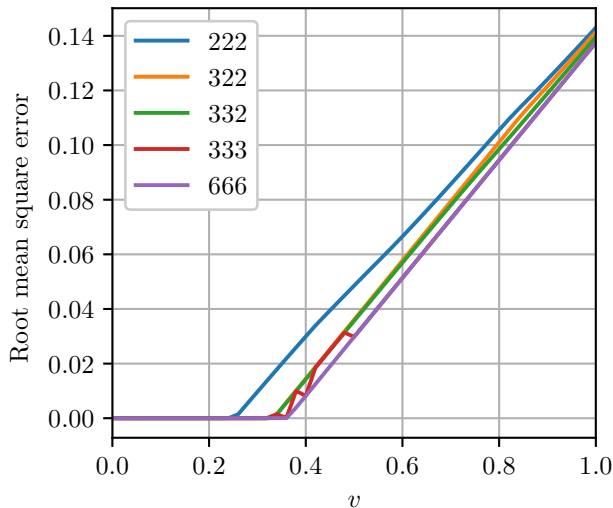


FIG. 6. Optimization error as a function of the visibility of the GHZ distribution. For visibilities $v \gtrsim 0.36$, the error reaches values very close to zero, indicating that these behaviours are network local. For visibilities $v \lesssim 0.36$, the solver can no longer achieve low optimization errors, indicating that these behaviours are most likely not network local.

function arrays are very close to 0 or 1. By fixing those entries and solving for the other ones with the use of a symbolic computation package, we were able to find the following models for each cardinality triplet.

For $(c_\alpha, c_\beta, c_\gamma) = (2, 2, 2)$, the following model reproduces the GHZ distribution with visibility $v = 1/4$:

$$p_\alpha[\alpha] = p_\beta[\beta] = p_\gamma[\gamma] = \left[\frac{1}{2} \quad \frac{1}{2}\right] \quad (22a)$$

$$p_a[0, \beta, \gamma] = p_b[0, \gamma, \alpha] = p_c[0, \alpha, \beta] = \begin{bmatrix} 0 & \frac{1}{2} \\ \frac{1}{2} & 1 \end{bmatrix} \quad (22b)$$

Lower visibilities can be achieved if the parties follow this strategy with some probability or just produce uniformly distributed random outputs, otherwise.

For $(c_\alpha, c_\beta, c_\gamma) = (3, 2, 2)$, the following model reproduces the target distribution for all visibilities in the range $0 \leq v \leq 1/3$:

$$p_\alpha[\alpha] = \left[\frac{v}{2} \quad 1-v \quad \frac{v}{2}\right], \quad (23a)$$

$$p_\beta[\beta] = \left[\frac{1}{2} \quad \frac{1}{2}\right], \quad (23b)$$

$$p_\gamma[\gamma] = \left[\frac{1}{2} \quad \frac{1}{2}\right], \quad (23c)$$

$$p_a[0, \beta, \gamma] = \begin{bmatrix} \frac{1-3v}{2(1-v)} & \frac{1}{2} \\ \frac{1}{2} & \frac{1+v}{2(1-v)} \end{bmatrix}, \quad (23d)$$

$$p_b[0, \gamma, \alpha] = \begin{bmatrix} 1 & 0 & 0 \\ 1 & 1 & 0 \end{bmatrix}, \quad (23e)$$

$$p_c[0, \alpha, \beta] = \begin{bmatrix} 1 & 1 \\ 0 & 1 \\ 0 & 0 \end{bmatrix}. \quad (23f)$$

For $(c_\alpha, c_\beta, c_\gamma) = (3, 3, 3)$, we found the following model with parameters a and b :

$$p_\alpha[\alpha] = p_\beta[\beta] = p_\gamma[\gamma] = [a \quad b \quad 1-a-b], \quad (24a)$$

$$p_a[0, \beta, \gamma] = p_b[0, \gamma, \alpha] = p_c[0, \alpha, \beta] = \begin{bmatrix} 0 & 1 & 0 \\ 1 & 1 & 0 \\ 0 & 0 & 0 \end{bmatrix}. \quad (24b)$$

By setting $a \approx 0.454$ and $b \approx 0.386$, the unique roots in the interval $[0, 1]$ of the polynomials $12a^4 - 8a^3 + 6a^2 - 1$ and $4b^4 - 8b + 3$, respectively, the model reproduces the behaviour of equation (21) with visibility

$$v = 2b - 3 + \frac{1}{b} \approx 0.362.$$

This visibility is the largest real root of the polynomial $3v^4 + 28v^3 + 66v^2 - 36v + 3$. Since the model is symmetric with respect to the parties, lower visibilities can be achieved in the same manner of the $(2, 2, 2)$ models, that is, with appropriate white noise admixture.

These findings lead us to conjecture that the critical visibilities for GHZ distribution in the context of each cardinality triplet are $v_c^{222} = 1/4$, $v_c^{322} = 1/3$ and $v_c^{333} \approx 0.362$, matching our expectations from figure 6. We also conjecture that no further increases in the critical visibility are possible by considering models with cardinalities higher than $(3, 3, 3)$, as figure 6 suggests.

It is important to stress out the fact that although the GHZ distribution is named after the well known quantum state, this does not mean that it is realizable with visibility $v = 1$ in the triangle scenario using quantum sources, because the GHZ state exhibits tripartite entanglement, while we are only allowed to use bipartite sources in the triangle network. Indeed, using inequality (34) of [22], it can be proven that even using quantum sources, $v \leq 0.5$. This indicates that it may be possible for noisy GHZ distributions of quantum mechanical origin to be network nonlocal (for $0.362 < v \leq 0.5$).

What we did in the above was to try to fit a network local model to a distribution $p = vp_1 + (1-v)p_0$, where p_1 is the GHZ distribution and p_0 is white noise. If the distributions p_1 and p_0 exhibit symmetry between the three parties (as is the case), and the network-local set is not too much concave, we expect the local model for $v = v_c$ to be the solution found by the optimization routine even when $v > v_c$. In this situation, it is impossible to find a local model, but the model that best approximates the target distribution is the one for $v = v_c$. This is expected at least in close proximity of v_c . If that is the case, the root mean square error in the probabilities is:

$$\begin{aligned}
E &= \left\{ \frac{1}{8} \sum_{a,b,c} [p_c(a,b,c) - p^*(a,b,c)]^2 \right\}^{1/2} \\
&= \left\{ \frac{1}{8} \sum_{a,b,c} [p_0(a,b,c) - p_1(a,b,c)]^2 \right\}^{1/2} (v - v_c).
\end{aligned} \tag{25}$$

We see that the root mean square error should increase linearly with v , as shown in figure 6. Indeed, for the GHZ distribution, equation (25) reduces to

$$E = \frac{\sqrt{3}}{8}(v - v_c) \approx 0.2165(v - v_c),$$

which matches the slope seen in figure 6 for models with $(c_\alpha, c_\beta, c_\gamma) = (6, 6, 6)$ (also for models with $c_\alpha = c_\beta = c_\gamma \geq 3$).

B. W distribution

Let us consider another target behaviour, the so called W distribution, named after the homonymous quantum state [23], mixed with uniformly distributed random noise:

$$p(a, b, c) = \begin{cases} \frac{v}{3} + \frac{1-v}{8} & \text{if } a + b + c = 1 \\ \frac{1-v}{8} & \text{otherwise.} \end{cases} \tag{26}$$

The root mean square error in the probabilities can be seen in figure 7, for the same cardinalities as in the previous subsection. Unlike what happened with the GHZ distribution, the cardinalities $(c_\alpha, c_\beta, c_\gamma) = (3, 2, 2)$ seem to be enough to solve the problem. Again, we see some oscillations of the $(3, 2, 2)$ curve between those of the triplets $(2, 2, 2)$ and $(6, 6, 6)$. By running the optimization for v close to the critical value, we obtain a model with β and γ being nearly identically distributed and Bob and Charles having nearly deterministic response functions. By forcing these constraints and solving for the other parameters, we were able to find the following model for

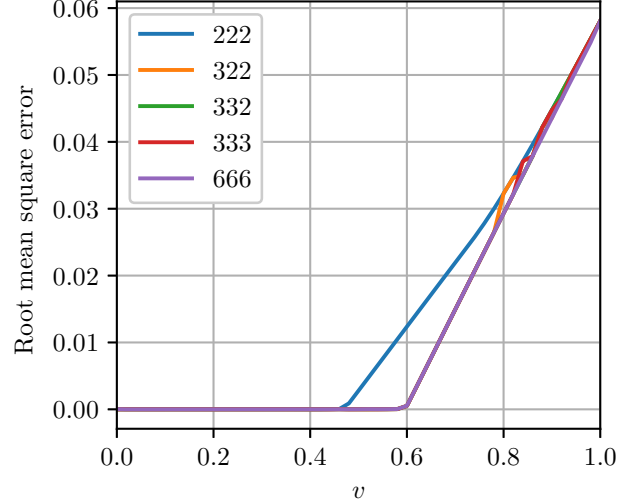


FIG. 7. Optimization error as a function of the visibility of the W distribution. For visibilities $v \lesssim 0.6$, the error reaches values very close to zero, indicating that these behaviours are network local. For visibilities $v \gtrsim 0.6$, the solver can no longer achieve low optimization errors, indicating that these behaviours are most likely not network local.

$v \in [0, v_c]$:

$$p_\alpha[\alpha] = \left[\frac{3+v}{12} - \frac{1-v}{4u} \left(\frac{1-v}{4} \right) \left(1 + \frac{1}{u} \right)^2 \frac{3+v}{12} - \frac{1-v}{4u} \right] \tag{27a}$$

$$p_\beta[\beta] = p_\gamma[\gamma] = \left[\frac{u}{1+u} \frac{1}{1+u} \right] \tag{27b}$$

$$p_a[0, \beta, \gamma] = \left[\frac{1}{2} \frac{3+v}{6} + \frac{uv(9-v)}{18(1-v)} \frac{3+v}{6} + \frac{uv(9-v)}{18(1-v)} \frac{3(1-v)}{2(3+v)} \right] \tag{27c}$$

$$p_b[0, \gamma, \alpha] = \begin{bmatrix} 1 & 0 & 0 \\ 1 & 1 & 0 \end{bmatrix} \tag{27d}$$

$$p_c[0, \alpha, \beta] = \begin{bmatrix} 0 & 0 \\ 0 & 1 \\ 1 & 1 \end{bmatrix}, \tag{27e}$$

where $u = \sqrt{3(1-v)/(3+v)}$. This model breaks down for $v > v_c$ because the off-diagonal elements of Alice's response function become larger than 1. By constraining these elements to be equal to 1, one finds that v_c is the root of the polynomial $4v^4 - 30v^3 + 63v^2 + 108v - 81$ which is within the interval $[0, 1]$, i.e. $v_c \approx 0.5966$, matching our expectations from figure 7.

As was the case of the GHZ distribution, notice that the W distribution with $v = 1$ is not achievable using quantum bipartite sources in the triangle scenario. Indeed, it has been proven that quantum strategies cannot achieve visibilities higher than $v = 6 - 3\sqrt{3} \approx 0.8039$ [24]. These results also leave room for quantum-mechanical noisy W distributions to present non-trilocality.

The slope of figure 7 for the region $v > v_c$ can be analyzed in the same way as we did in the previous subsection. For the W distribution, equation (25) becomes

$$E = \frac{\sqrt{15}}{24}(v - v_c) \approx 0.1614(v - v_c).$$

This slope matches the one obtained numerically in figure 7 for models with $(c_\alpha, c_\beta, c_\gamma) = (6, 6, 6)$ (also for models with $c_\alpha = c_\beta + 1 = c_\gamma + 1 \geq 3$)

C. EJM distribution

Finally, we consider the so called Elegant Joint Measurement (EJM) distribution, that can be generated by a quantum strategy [25]. This behaviour is conjectured to be nonlocal, so a natural question is: how much noise must we mix with the EJM distribution so that it becomes network local? The target distribution is:

$$p(a, b, c) = v p_{EJM}(a, b, c) + \frac{1-v}{64}. \quad (28)$$

For the triangle network with four outputs, the full cardinalities $c_\alpha = c_\beta = c_\gamma = 60$ render the optimization run time prohibitively large. However, some insight into the critical visibility for a given distribution can be gained by exploring models with lower cardinalities. We have tested for all possible cardinalities up until $c_\alpha = c_\beta = c_\gamma = 7$. The tables below show the maximum values of v for which the numerical optimization procedure could find a model with root mean square error less than 1×10^{-4} . We believe these should serve as rough estimates for the critical visibility for network local behaviours constrained by the tested cardinalities. Notice that the target distribution is symmetric with respect to the three parties, so we can without loss of generality assume henceforth that $c_\alpha \geq c_\beta \geq c_\gamma$ (that justifies the blank spaces in the tables).

$c_\gamma = 2$

$c_\alpha \backslash c_\beta$	2	3	4	5	6	7
2	0.005	0.007	0.009	0.012	0.012	0.012
3		0.012	0.014	0.014	0.014	0.014
4			0.018	0.018	0.018	0.018
5				0.018	0.018	0.018
6					0.018	0.018
7						0.018

$c_\gamma = 3$

$c_\alpha \backslash c_\beta$	3	4	5	6	7
3	0.014	0.018	0.018	0.018	0.018
4		0.025	0.025	0.025	0.025
5			0.025	0.025	0.025
6				0.025	0.025
7					0.025

$c_\gamma = 4$

$c_\alpha \backslash c_\beta$	4	5	6	7
4	0.318	0.397	0.397	0.397
5		0.398	0.399	0.399
6			0.399	0.400
7				0.400

$c_\gamma = 5$

$c_\alpha \backslash c_\beta$	5	6	7
5	0.398	0.402	0.403
6		0.402	0.405
7			0.405

$c_\gamma = 6$

$c_\alpha \backslash c_\beta$	6	7
6	0.404	0.405
7		0.405

$c_\gamma = 7$

$c_\alpha \backslash c_\beta$	7
7	0.405

As can be noticed by inspecting the tables, the smaller cardinality c_γ seems to be the most constraining factor to the maximum visibility that one can achieve using network local models. Furthermore, we see a significant increase in the critical visibility from values close to zero to 0.318 for cardinalities $(c_\alpha, c_\beta, c_\gamma) = (4, 4, 4)$. After that, there is another increase in the critical visibility to 0.397 for $(c_\alpha, c_\beta, c_\gamma) = (5, 4, 4)$, and then the increments become fairly marginal. These results show that for visibilities up to approximately 0.4, the EJM distribution mixed with uniform random noise is trilocal. It is always possible that this range can be widened by utilising larger cardinalities, but the approximate value of 0.4 is a lower bound for the true critical visibility. It can be regarded as an initial candidate to the true critical visibility, regardless of the hidden-variable cardinalities.

V. CLOSING REMARKS

A tool for finding explicit models in network scenarios with finite hidden variable cardinality was developed. We hope it will be useful to the community interested in advancing the understanding of network-nonlocality. In this paper, we have used the tool to find the critical visibilities of the GHZ, W, and EJM distributions, when mixed with uniform random noise. For the GHZ and W distributions, we found 4th degree polynomials

whose roots are conjectured to be the critical visibilities, along with the exact network-local strategies that generate these behaviours. For the EJM distribution, we found only numerical estimates of the critical visibility by looking at models with reduced cardinalities for the hidden variables.

The first area where future work could be done is in trying to improve the execution time and accuracy of the numerical routine. In the implementation used to generate figures 3, 4, 6 and 7, each time the solver attempts to find a local model, the initial guess is completely random. So if an acceptable model was found for one point, this achievement was not taken into account when investigating neighbouring points. Doing this could help expedite calculations and also reduce the probability of failure when trying to find a model for a point which is network-local. In certain affine subspaces, symmetry could also be an important factor. For example, in the subspace of figure 3, the symmetries $I \rightarrow -I$ and $J \rightarrow -J$ correspond to simple relabelings of outputs and inputs. So there is actually no need to employ computing power in more than one quadrant.

An interesting issue is the matter of cardinality reduction in the hidden variables. As we saw in section IV, the behaviour obtained by the GHZ distribution mixed with the uniform distribution with critical visibility could be

obtained with cardinalities $c_\alpha = c_\beta = c_\gamma = 3$, although the upper bound provided by [14] is $c_\alpha = c_\beta = c_\gamma = 6$. On the other hand, for the W distribution, $(c_\alpha, c_\beta, c_\gamma) = (3, 2, 2)$ seems to be sufficient to reproduce the critical behaviour. What determines when such reductions are possible and by how much? An investigation of this question could shed light on network nonlocality.

The fact that the critical visibilities of both the GHZ and W distributions are conjectured to be roots of 4th degree polynomials tells us that there would be polynomial Bell inequalities of the same degree (at least) for the triangle scenario with binary outputs that still eludes us. The search for these inequalities is also an exciting possible avenue of future research.

ACKNOWLEDGMENTS

This work received financial support from the Brazilian agencies Coordenação de Aperfeiçoamento de Pessoal de Nível Superior (CAPES), Fundação de Amparo à Ciência e Tecnologia do Estado de Pernambuco (FACEPE), Conselho Nacional de Desenvolvimento Científico e Tecnológico through its program CNPq INCT-IQ (Grant 465469/2014-0), and Fundação de Amparo à Pesquisa do Estado de São Paulo (FAPESP - Grant 2021/06535-0).

-
- [1] J. S. Bell, On the einstein podolsky rosen paradox, *Physics Physique Fizika* **1**, 195 (1964).
 - [2] G. Svetlichny, Distinguishing three-body from two-body nonseparability by a bell-type inequality, *Phys. Rev. D* **35**, 3066 (1987).
 - [3] J.-D. Bancal, N. Brunner, N. Gisin, and Y.-C. Liang, Detecting genuine multipartite quantum nonlocality: A simple approach and generalization to arbitrary dimensions, *Phys. Rev. Lett.* **106**, 020405 (2011).
 - [4] R. Gallego, L. E. Würflinger, A. Acín, and M. Navascués, Operational framework for nonlocality, *Phys. Rev. Lett.* **109**, 070401 (2012).
 - [5] J.-D. Bancal, J. Barrett, N. Gisin, and S. Pironio, Definitions of multipartite nonlocality, *Phys. Rev. A* **88**, 014102 (2013).
 - [6] A. K. Ekert, Quantum cryptography based on bell's theorem, *Phys. Rev. Lett.* **67**, 661 (1991).
 - [7] H. Buhrman, R. Cleve, S. Massar, and R. de Wolf, Nonlocality and communication complexity, *Rev. Mod. Phys.* **82**, 665 (2010).
 - [8] N. Brunner, D. Cavalcanti, S. Pironio, V. Scarani, and S. Wehner, Bell nonlocality, *Reviews of Modern Physics* **86**, 419 (2014).
 - [9] V. Scarani, *Bell nonlocality* (Oxford Graduate Texts, 2019).
 - [10] C. Branciard, N. Gisin, and S. Pironio, Characterizing the nonlocal correlations created via entanglement swapping, *Physical review letters* **104**, 170401 (2010).
 - [11] T. Fritz, Beyond bell's theorem: correlation scenarios, *New Journal of Physics* **14**, 103001 (2012).
 - [12] M.-O. Renou, E. Bäumer, S. Boreiri, N. Brunner, N. Gisin, and S. Beigi, Genuine quantum nonlocality in the triangle network, *Physical review letters* **123**, 140401 (2019).
 - [13] A. Tavakoli, A. Pozas-Kerstjens, M.-X. Luo, and M.-O. Renou, Bell nonlocality in networks, arXiv preprint arXiv:2104.10700 (2021).
 - [14] D. Rosset, N. Gisin, and E. Wolfe, Universal bound on the cardinality of local hidden variables in networks, arXiv preprint arXiv:1709.00707 (2017).
 - [15] D. Collins and N. Gisin, A relevant two qubit bell inequality inequivalent to the CHSH inequality, *Journal of Physics A: Mathematical and General* **37**, 1775 (2004).
 - [16] P. Virtanen, R. Gommers, T. E. Oliphant, M. Haberland, T. Reddy, D. Cournapeau, E. Burovski, P. Peterson, W. Weckesser, J. Bright, S. J. van der Walt, M. Brett, J. Wilson, K. J. Millman, N. Mayorov, A. R. J. Nelson, E. Jones, R. Kern, E. Larson, C. J. Carey, Í. Polat, Y. Feng, E. W. Moore, J. VanderPlas, D. Laxalde, J. Perktold, R. Cimrman, I. Henriksen, E. A. Quintero, C. R. Harris, A. M. Archibald, A. H. Ribeiro, F. Pedregosa, P. van Mulbregt, and SciPy 1.0 Contributors, SciPy 1.0: Fundamental Algorithms for Scientific Computing in Python, *Nature Methods* **17**, 261 (2020).
 - [17] R. Byrd, M. Hribar, and J. Nocedal, An interior point algorithm for large-scale nonlinear programming, *SIAM Journal on Optimization* **9**, 877 (1999).
 - [18] T. Kriváchy, Y. Cai, D. Cavalcanti, A. Tavakoli, N. Gisin, and N. Brunner, A neural network oracle for quantum nonlocality problems in networks, *npj Quantum Information* **6**, 70 (2020).
 - [19] C. Branciard, D. Rosset, N. Gisin, and S. Pironio, Bilocal

- versus nonbilocal correlations in entanglement-swapping experiments, *Physical Review A* **85**, 032119 (2012).
- [20] R. F. Werner and M. M. Wolf, All-multipartite bell-correlation inequalities for two dichotomic observables per site, *Physical Review A* **64**, 10.1103/physreva.64.032112 (2001).
- [21] D. M. Greenberger, M. A. Horne, A. Shimony, and A. Zeilinger, Bell's theorem without inequalities, *American Journal of Physics* **58**, 1131 (1990), <https://doi.org/10.1119/1.16243>.
- [22] E. Wolfe, R. W. Spekkens, and T. Fritz, The inflation technique for causal inference with latent variables, *Journal of Causal Inference* **7** (2019).
- [23] W. Dür, G. Vidal, and J. I. Cirac, Three qubits can be entangled in two inequivalent ways, *Phys. Rev. A* **62**, 062314 (2000).
- [24] E. Wolfe, A. Pozas-Kerstjens, M. Grinberg, D. Rosset, A. Acín, and M. Navascués, Quantum inflation: A general approach to quantum causal compatibility, *Phys. Rev. X* **11**, 021043 (2021).
- [25] N. Gisin, The elegant joint quantum measurement and some conjectures about n-locality in the triangle and other configurations, arXiv preprint arXiv:1708.05556 (2017).